RESEARCH ARTICLE

Open Access

Polarization-entangled photon-pair source with van der Waals 3R-WS$_2$ crystal

Jiangang Feng[1†] , Yun-Kun Wu[2,3,4*†], Ruihuan Duan[5†], Jun Wang[6], Weijin Chen[1], Jiazhang Qin[1], Zheng Liu[5], Guang-Can Guo[2,3,4], Xi-Feng Ren[2,3,4*] and Cheng-Wei Qiu[1*]

Abstract

Ultracompact entangled photon sources are pivotal to miniaturized quantum photonic devices. Van der Waals (vdW) nonlinear crystals promise efficient photon-pair generation and on-chip monolithic integration with nanophotonic circuitry. However, it remains challenging to generate maximally entangled Bell states of photon pairs with high purity, generation rate, and fidelity required for practical applications. Here, we realize a polarization-entangled photon-pair source based on spontaneous parametric down conversion in an ultrathin rhombohedral tungsten disulfide (3R-WS$_2$) crystal. This vdW entangled photonic source exhibits a high photon-pair purity with a coincidence-to-accidental ratio of above 800, a generation rate of 31 Hz, and two maximally polarization-entangled Bell states with fidelities exceeding 0.93 and entanglement degree over 0.97. These results stem from scalable optical nonlinearity, enhanced second-order susceptibility by electronic transitions, and a well-defined symmetry-enabled selection rule inherent in 3R-WS$_2$. Our polarization entangled photon source can be integrated with photonic structures for generating more complex entangled states, thus paving an avenue for advanced quantum photonic systems toward computation and metrology.

†Jiangang Feng, Yun-Kun Wu and Ruihuan Duan have authors contributed equally to this work.

*Correspondence:
Yun-Kun Wu
wuyk123@mail.ustc.edu.cn
Xi-Feng Ren
renxf@ustc.edu.cn
Cheng-Wei Qiu
chengwei.qiu@nus.edu.sg
[1] Department of Electrical and Computer Engineering, National University of Singapore, Singapore 117583, Singapore
[2] CAS Key Laboratory of Quantum Information, University of Science and Technology of China, Hefei 230026, China
[3] CAS Center for Excellence in Quantum Information and Quantum Physics, University of Science and Technology of China, Hefei 230026, China
[4] Hefei National Laboratory, University of Science and Technology of China, Hefei 230088, China
[5] School of Materials Science and Engineering, Nanyang Technological University, Singapore 639798, Singapore
[6] Department of Optical Science and Engineering, and Shanghai Frontiers Science Research Base of Intelligent Optoelectronics and Perception, Fudan University, Shanghai 200433, China

1 Introduction

Entangled photon pairs are fundamental in quantum science, escalating our understanding of quantum nonlocality through the violation of Bell inequalities [1], and playing a pivotal role in modern quantum technologies for computation, communication, and metrology [2]. Spontaneous parametric down-conversion (SPDC), a second-order nonlinear optical process that splits a high-energy photon into a pair of correlated photons, is deployed to generate photon pairs with entanglement across diverse degrees of freedom (DoFs) like polarization [3], path [4], spatial mode [5], and time-energy [6]. Among these DoFs, polarization has been widely adopted to create maximally entangled Bell states in bulk SPDC sources [3, 7]. However, their bulk nature impedes integration into compact integrated quantum systems, such as quantum photonic circuits for computation [8, 9], and quantum microscopy for imaging [10].

Van der Waals (vdW) crystals, featuring giant non-linear susceptibilities and subwavelength thickness, are promising for integrated quantum photonics [11–13]. For efficient SPDC, it is essential that the optical non-linearity in vdW crystals can scale with their thickness, which requires preserved lattice non-centrosymmetry as layers are being stacked. In this context, hexagonal (2H) prototype transition-metal dichalcogenides (TMDCs) have been excluded due to their vanishing nonlinearity in each bilayer [14, 15]. Notably, the highly distorted crystal $NbOCl_2$ has been demonstrated as efficient for correlated photon-pair generation in ultrathin structures [12]. In principle, these ultrathin nonlinear crystals hold significant promise for integration with nanophotonic components, such as waveguides [16], resonators [17], and metasurfaces [4, 18, 19], to generate complex entangled photonic states with high tunability in a compact footprint. Unfortunately, restricted by low lattice symmetry, these vdW crystals often exhibit a complicated nonlinear susceptibility tensor, resulting in intricate optical fields after nonlinear conversion and ill-defined entanglement in generated photon-pairs [12]. Thus, maximally entangled Bell states have not been realized in vdW materials. For practical applications, a compact entangled photon source must satisfy three rigorous requirements: (i) a well-defined quantum entanglement, (ii) broken lattice centrosymmetry for scalable nonlinearity, (iii) large second-order susceptibilities for enhancing photon-pair generation rate.

Our work reports an ultracompact source of polarization-entangled photon pairs with a 350-nm-thick rhombohedral 3R-WS_2 crystal, which meets the three above-mentioned requirements simultaneously. The broken centrosymmetry along the layer-stacking direction enables scalable optical nonlinearity, while the preserved in-plane three-fold rotational symmetry facilitates a well-defined nonlinear optical selection rule. This includes a flipped spin angular momentum (SAM) during second-order nonlinear conversion, allowing polarization-entangled photon-pair states in SPDC process. By resonant coupling with electronic levels in 3R-WS_2 without introducing photoluminescence (PL) noise, we achieve a substantially enhanced second-order susceptibility for efficient SPDC. This strategy enables efficient photon-pair generation with a high coincidence-to-accidental ratio exceeding 800, and a generation rate of 31 Hz. Leveraging the symmetry-enabled selection rule, two maximally entangled Bell states have been prepared with high fidelities above 0.93 and entanglement degrees, quantified by concurrences, exceeding 0.97. These findings pave the way for the on-chip monolithic integration of 3R-WS_2 with nanophotonic structures, leading to miniaturized entangled photon-pair sources capable of generating complex states with high tunability.

2 Results and discussion

The experimental realization of polarization-entangled photon pair sources relies on the judicious selection of 3R-WS_2 with a $R3m$ space group. 3R-WS_2 presents ABC stacking along the out-of-plane orientation, a feature that breaks inversion symmetry from the monolayer to bulk crystal. Thereby second-order optical nonlinearity (Fig. 1a) can be scaled up with the thickness. In contrast to the highly distorted lattices such as $NbOCl_2$, 3R-WS_2 exhibits an in-plane C_{3v} symmetry with three-fold rotational axes and mirror planes (Fig. 1b). Such symmetry simplifies the second-order susceptibility tensor, leaving a nonvanishing element $\chi_{yyy}^{(2)} = -\chi_{yxx}^{(2)} = -\chi_{xxy}^{(2)} = -\chi_{xyx}^{(2)} = \chi^{(2)}$ for transverse electric fields. Under this tensor configuration, the non-linear optical process adheres to a well-defined selection rule: a circularly polarized pump yields up/down-converted photons with an opposite circular polarization [7, 20]. This spin angular momentum (SAM) flipping correlates with total SAM conservation in the non-linear process, where the SAM mismatching between the pump and emitted photons is compensated by the crystal with the three-fold rotational symmetry [21]. In the SPDC process, this selection rule enables the generation of photon pairs $|LL\rangle_{s,i}$ and $|RR\rangle_{s,i}$ with correlated circular polarizations, leveraging pumps of $|R\rangle_{pump}$ and $|L\rangle_{pump}$, respectively, where R/L denotes right/left circularly polarized states (Fig. 1a). By coherent superposition of these states, we have successfully prepared a polarization-entangled photon-pair state in the form of $1/\sqrt{2}(|LL\rangle_{s,i} + e^{i2\alpha}|RR\rangle_{s,i})$ through a linearly polarized pump $1/\sqrt{2}(|R\rangle_{pump} + e^{i2\alpha}|L\rangle_{pump})$ at an angle α with respect to armchair direction in 3R-WS_2. Although 2H-type TMDC monolayers with D_{3h} symmetry present a similar optical selection rule, their atomically short interaction length renders the probabilistic SPDC process unobservable, highlighting the unique advantage of the 3R stacking [15].

We first conduct second harmonic generation (SHG) measurements to elucidate the second-order nonlinearity of 3R-WS_2. The pump wavelength is centered at 914 nm, producing SHG at 457 nm. Our power-dependent measurements reveal that SHG intensity follows the expected quadratic increasement with the pump power (Fig. S1). Figure 1c depicts SHG mapping of a 260-nm-thick flake, where the bright SHG emission confirms the preservation of noncentrosymmetry in the stacked 3R-WS_2 layers. The in-plane lattice symmetry is further analyzed through polarization-dependent SHG, involving the
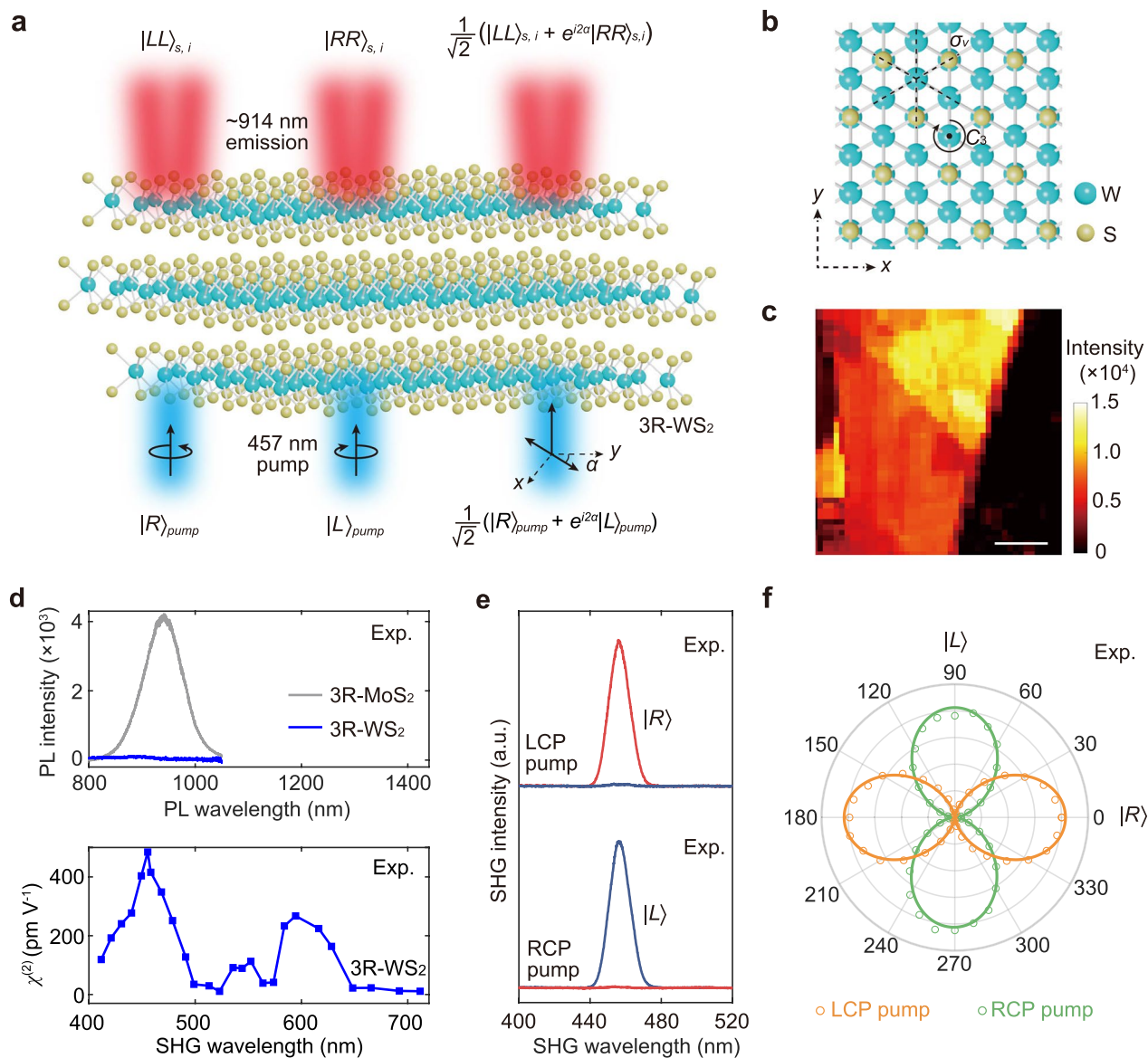
Fig. 1 Generation of polarization-entangled photon pairs in 3R-WS$_2$. **a**, Conceptual illustration depicting the generation of polarization-entangled photon pairs in thin crystals of 3R-WS$_2$. Leveraging the C_{3v} symmetry of 3R-WS$_2$, a nonlinear optical selection rule is established: $|R\rangle_{pump} \rightarrow |LL\rangle_{s,i}$, $|L\rangle_{pump} \rightarrow |RR\rangle_{s,i}$. This empowers a polarization-entangled photonic state $1/\sqrt{2}(|LL\rangle_{s,i} + e^{i2\alpha}|RR\rangle_{s,i})$ through a linearly polarized pump $1/\sqrt{2}(|R\rangle_{pump} + e^{i2\alpha}|L\rangle_{pump})$, where α is the polarization angle relative to the y axis, and y represents the armchair direction. **b**, Schematic representation of the C_{3v} symmetry in 3R-WS$_2$, where C_3 and σ_v denote the three-fold rotational symmetry axis and the mirror symmetry plane, respectively. **c**, SHG mapping at 457 nm, achieved by pumping with a 914 nm laser. Scale bar, 20 μm. **d**, Spectral dependence of $\chi^{(2)}$ in 3R-WS$_2$ (bottom), and comparison of the PL spectra of our own 3R-WS$_2$ and 3R-MoS$_2$ (top). All data are experimental measurements. **e**, Circular polarization-resolved SHG spectra illustrate the nonlinear optical selection rule with counter-circularly polarized SHG signals. **f**, SHG intensity as a function of the angle of a quarter-wave plate analyzer in front of the detector

rotation of 3R-WS$_2$ relative to co-linearly polarized pump and analyzer. As shown in Fig. S2, the SHG intensity displays a characteristic six-lobed pattern, consistent with the C_{3v} crystal symmetry.

An efficient and high-quality entangled photon-pair source requires the following conditions simultaneously:

(1) a high second-order susceptibility $\chi^{(2)}$ for high-rate photon-pair generation, and (2) a minimized PL background for strong quantum correlation. In nonlinear crystals, $\chi^{(2)}$ can be substantially enhanced when fundamental or SH photons resonantly couple with electronic transitions [11]. However, this strategy often leads to

random PL emissions that is generally a lot more significant than SPDC process, impairing quantum correlation of photon pairs. For instance, in 3R-MoS$_2$, selecting a pump wavelength in the 450–500 nm range can resonate with electronic transitions, thereby increasing $\chi^{(2)}$ [11]. Nevertheless, as indicated by our PL measurements, broadband PL emissions in 600–1050 nm range, stemming from exciton recombination and indirect bandgap transitions, demonstrate spectral overlap with the down-converted photon pairs within the 900–1000 nm range (Fig. 1d, S3). This broadband PL restricts the potential for exploiting enhanced $\chi^{(2)}$ in 3R-MoS$_2$. It is important to note that the resonance enhancement of $\chi^{(2)}$ is constrained by losses of pump energy due to the linear absorption process, which necessitates the exploration of materials with lower absorption coefficients in future research.

The SHG excitation spectrum of our 3R-WS$_2$ reveals two distinct wavelength ranges, 420–490 nm and 580–630 nm, with significantly higher $\chi^{(2)}$ values owing to electronic transitions. We further confirm these transitions through reflectance, absorption, and PL spectra of 3R-WS$_2$ (Fig. S3, S4). We observe three absorption peaks, labeled as A, B, and C in order of increasing energy (Fig. S4). Peaks A and B can be attributed to excitonic transitions at the K and K' valleys, while peak C around 460 nm is contributed by transitions in a high joint density of states (JDOS) region [22]. This high JDOS region is formed by the 'band nesting' effect [23], where parallel conduction and valence bands produce even higher $\chi^{(2)}$ than excitonic transitions at the band edge. Notably, the maximum $\chi^{(2)}$ value can reach 480 pm V^{-1} at SHG wavelength of 457 nm in 3R-WS$_2$, representing a significant improvement over the less than 5 pm V^{-1} observed in bulk nonlinear crystals like beta-barium borate and potassium dihydrogen phosphate [24]. This high $\chi^{(2)}$ facilitates observable SPDC in subwavelength thin nanoflakes. The PL spectrum of 3R-WS$_2$ displays emissions ranging from 600 to 800 nm, corresponding to the exciton recombination, while PL signal is unobservable beyond 900 nm (Fig. 1d, S3). Therefore, we choose the pump wavelength at 457 nm, and down-converted photon pairs could consequently be generated at 914 nm with strongly enhanced $\chi^{(2)}$ and yet nearly no PL noise.

We conduct circular-polarization-resolved SHG measurements to elucidate the selection rule. When using a left circularly polarized (LCP) pump, we predominantly observe SHG in right circular polarization (RCP), and vice versa for an RCP pump (Fig. 1e). The degree of circular polarization, defined as $(I_{RCP}-I_{LCP})$ / $(I_{RCP}+I_{LCP})$, exhibits absolute values exceeding 0.95 for both RCP and LCP pumps (Fig. 1f). This demonstrates that the C_{3v}

symmetry of the 3R-WS$_2$ crystal facilitates a flip in SAM during the nonlinear process.

The enhanced $\chi^{(2)}$ in the absence of PL background, combined with the unique optical selection rule, motivates and allows us to explore its application in polarization-entangled photon-pair sources. We conduct quantum correlation and quantum-state tomography on a 350 nm thick 3R-WS$_2$ flake. Our experimental setup, illustrated in Fig. 2a, includes: (1) pumping down-converted photon pairs with a 457 nm continuous-wave laser, and (2) detecting them through two-photon coincidence events using single-photon detectors. The second-order correlation function is defined as $g^{(2)}(\tau) = \langle N_s(t)N_i(t+\tau)\rangle / \langle N_s(t)\rangle\langle N_i(t+\tau)\rangle$, where $N_{s,i}$ represents photon numbers registered at the signal and idler detectors, and τ is the delay time. Figure 2b shows typical twin-photon bunching at different pump powers. We observe a peak $g^{(2)}$ (0) value of 820 at 2.5 mW pump power, indicating an extremely high degree of quantum correlations in our vdW 3R-WS$_2$ photon-pair source.

We also grow another vdW crystal 3R-MoS$_2$ and carry out some comparative study. It is shown that $g^{(2)}$ (0) values for 3R-MoS$_2$ only exceed 2 at low pump powers. At 1 mW, $g^{(2)}$ (0) drops to 2.3, and twin photons become indiscernible from random emissions at 2.5 mW, suggesting unsustainable two-photon correlations in photon-pair sources with a PL background (Fig. 2b inset, Fig. S5). Though 3R-MoS$_2$ photon-pair sources operating at wavelengths above 1300 nm could largely suppress PL noise, the $\chi^{(2)}$-limited photon-pair generation rate inevitably includes random emissions during long-time integration, resulting in much lower $g^{(2)}$ (0) values below 10 [25]. The SPDC in our home-made 3R-WS$_2$ is further evidenced by inverse power dependence of $g^{(2)}$ (0) (Fig. 2c). Notably, even at a high pump power of 18.2 mW, robust quantum correlations are characterized by a $g^{(2)}$ (0) value of 49, which signifies highly pure correlated photon-pair generation distinct from classical random emissions.

The generation rate of this SPDC source is evaluated by its power-dependent coincidence rate, which shows a linear pump dependence, consistent with the SPDC mechanism (Fig. 2d). At a pump power of 18.2 mW, we achieve a high coincidence rate of 31.1 Hz, corresponding to a normalized generation rate of 1.71 Hz mW^{-1}. This generation rate is over 200 times higher than that of 3R-MoS$_2$ operating at 1576 nm [25], and comparable to the performance of state-of-the-art ultrathin vdW NbOCl$_2$ photon-pair sources (Table S1) [12]. However, NbOCl$_2$ cannot support well-defined quantum entanglement due to its lower lattice symmetry and resulting complicated $\chi^{(2)}$ tensor. To validate the selection rule in SPDC process, we pump photon pairs with a left/right
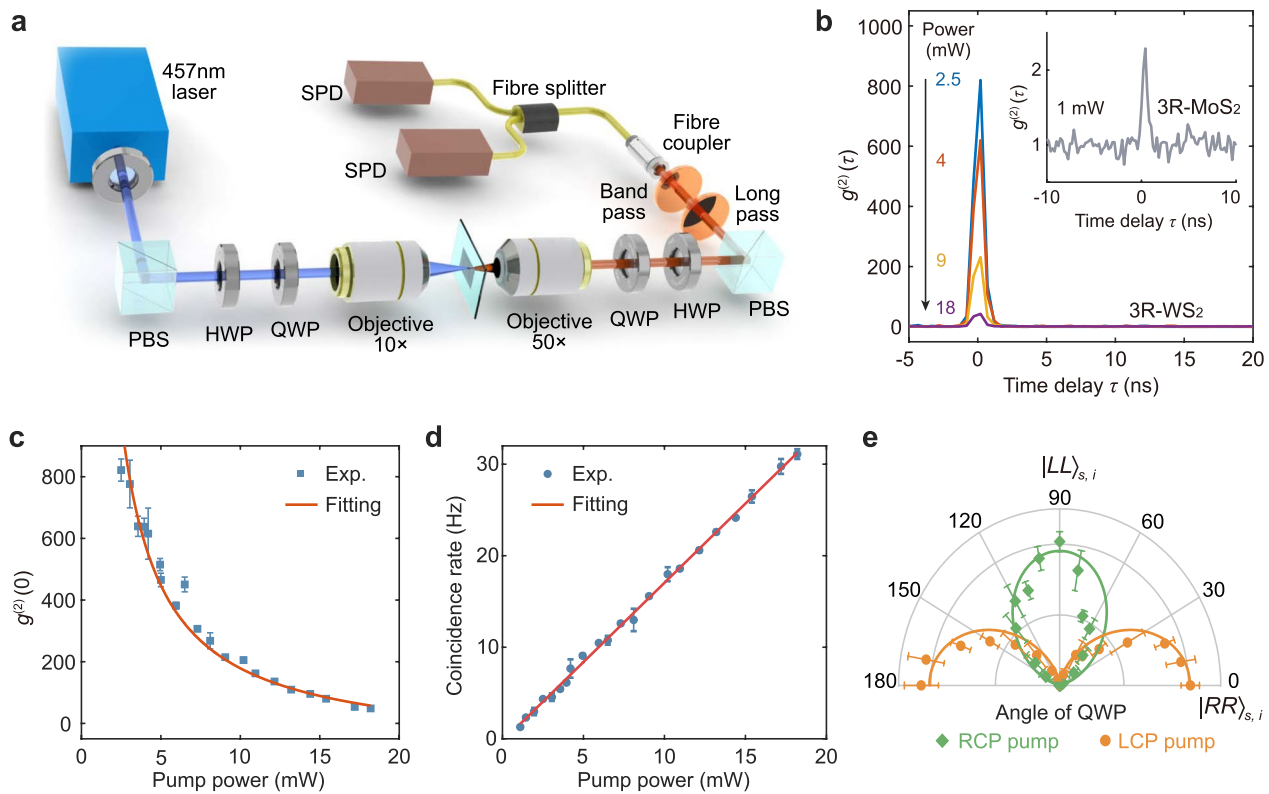
Fig. 2 SPDC for entangled photon-pair generation in 3R-WS$_2$. **a**, Sketch of experimental setup for SPDC measurements. **b**, Second-order correlation function $g^{(2)}(\tau)$ of 3R-WS$_2$ under different pump powers. Inset shows $g^{(2)}(\tau)$ of 3R-MoS$_2$ pumped by 457 nm laser at a power of 1 mW for comparison. **c**, Pump-power dependent $g^{(2)}(0)$ of 3R-WS$_2$. **d**, Coincidence rate as a function of pump power. **e**, Circular polarization analysis of photon pairs. Photon pairs are pumped by left-/right circularly polarized light and coincidence rate is recorded as a function of angle of the quarter-wave plate

circularly polarized light and measure coincidence rates at different angles of QWP. Figure 2e presents a distinct selection rule in SPDC process: $|L\rangle_{pump} \rightarrow |RR\rangle_{s,i}$ and $|R\rangle_{pump} \rightarrow |LL\rangle_{s,i}$, which is consistent with the SAM flipping measured by SHG.

To characterize quantum entanglement of generated photon pairs in 3R-WS$_2$, we perform full quantum state tomography and recover the density matrices of twin-photon states. We separate signal and idler photons by a polarization-independent beam splitter and project the twin-photon states onto different elements of the polarization basis (Fig. S6). The experimental demonstration of polarization entanglement is proceeded in the following two steps. First, we create photon pairs with LCP and RCP pumps, followed by 16 different measurements to recover the density matrix of each state (Fig. 3a, b). The experimental reconstructed density matrices are well consistent with ideal pure states of $|RR\rangle_{s,i}$ and $|LL\rangle_{s,i}$ characterized by fidelities F of 0.95 ± 0.03 and 0.93 ± 0.03, respectively.

Second, the nonlinear optical selection rule allows the superposition of circularly polarized photon-pair states to construct two maximally entangled Bell states. The general form of this polarization-entangled state is $1/\sqrt{2}(|LL\rangle_{s,i} + e^{i2\alpha}|RR\rangle_{s,i})$, achievable by a linearly polarized pump $1/\sqrt{2}(|R\rangle_{pump} + e^{i2\alpha}|L\rangle_{pump})$ at an angle α relative to the armchair direction of 3R-WS$_2$ (y-direction, as illustrated in Fig. 1b). At $\alpha = 0$, the state is expressed as $1/\sqrt{2}(|LL\rangle_{s,i} + |RR\rangle_{s,i})$, corresponding to the Bell state $1/\sqrt{2}(|HH\rangle_{s,i} - |VV\rangle_{s,i})$. Rotating the pump polarization to $\alpha = 90°$ transforms the photon-pair state to $1/\sqrt{2}(|LL\rangle_{s,i} - |RR\rangle_{s,i})$, which is another Bell state $1/\sqrt{2}(|HV\rangle_{s,i} + |VH\rangle_{s,i})$. In our experiments, these two states are prepared using linearly polarized pumps, and the recovered density matrices are displayed in Fig. 3c, d. The quantum tomography results align closely with ideal Bell states, exhibiting fidelities of 0.93 ± 0.05 and 0.96 ± 0.03, and concurrences C of 0.97 and 0.98 for the Bell states $1/\sqrt{2}(|HV\rangle_{s,i} + |VH\rangle_{s,i})$ and
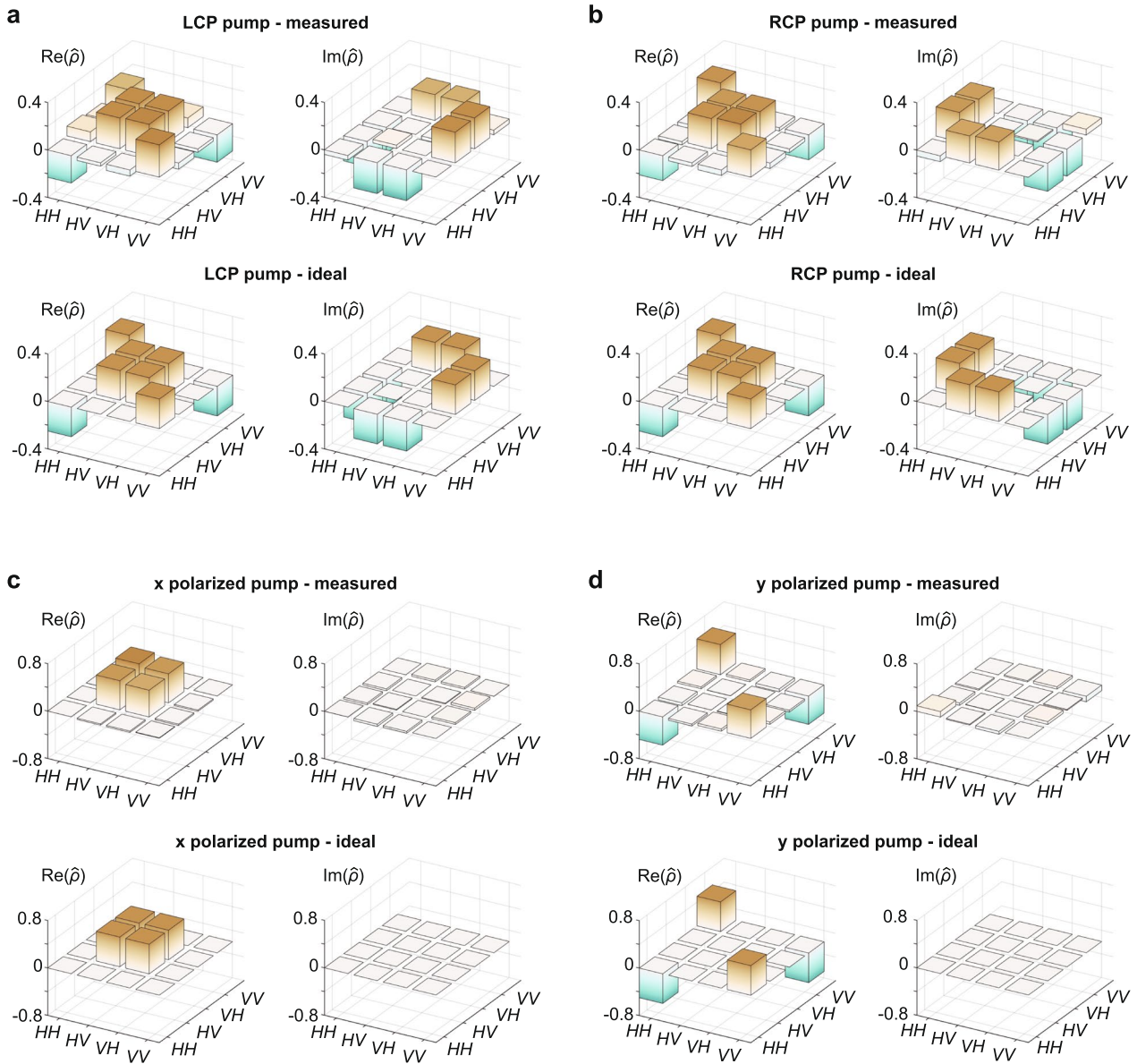
Fig. 3 Quantum state tomography of polarization-entangled photon pairs. A quantum state can be fully described by its density matrix $\hat{\rho}$. Measured and ideal density matrices with real (Re) and imaginary (Im) parts of (**a**) the $|RR\rangle_{s,i}$ state pumped by LCP, (**b**) the $|LL\rangle_{s,i}$ state pumped by RCP, (**c**) the Bell state $1/\sqrt{2}\left(|HV\rangle_{s,i} + |VH\rangle_{s,i}\right)$ pumped by linearly pumped light along x (zigzag) direction, (**d**) the Bell state $1/\sqrt{2}\left(|HH\rangle_{s,i} - |VV\rangle_{s,i}\right)$ pumped by linearly polarized light along y (armchair) direction

$1/\sqrt{2}\left(|HH\rangle_{s,i} - |VV\rangle_{s,i}\right)$, respectively. Consequently, we demonstrate two maximally entangled Bell states of photon pairs from 3R-WS$_2$, underscoring its potential for on-chip polarization-entangled photon-pair sources. It is worth noting that nonlinear crystals with other symmetries, such as GaP, can support polarization entanglement in one certain direction [26]. However, C_3 symmetric crystals can support continuously tunable polarization-entangled states with near-unity concurrence in SPDC process.

In conclusion, we report high-rate polarization-entangled photon pairs by SPDC in 3R-WS$_2$, a vdW crystal simultaneously allowing scalable second-order optical nonlinearity, a symmetry-enabled selection rule, and enhanced $\chi^{(2)}$ and nearly no PL noise at SPDC wavelengths. Despite a high $\chi^{(2)}$ in 3R-WS$_2$ facilitating a high generation rate among thin-film SPDC sources (Table S1), there remains a significant gap in the generation rate between vdW materials and well-developed bulk nonlinear crystals [3, 27], as well as quasi-phase-matched

waveguides and resonators [17, 28]. For practical applications in quantum optics systems, such as photonic quantum circuits [29], quantum walks [30], and free-space quantum teleportation [31], the 3R-WS$_2$ source still exhibits a 2–3 order of magnitude gap in the photon-pair generation rate. We anticipate that this gap can be closed by further integrating with resonant cavities and metasurfaces to enhance photon-pair generation efficiency [19], which is promising as the high refractive indices of TMDCs particularly benefit light confinement and nanophotonic design [32]. These resonant photonic structures can also enable the generation of more complex quantum states, such as orbital angular momentum entangled states [18] and spatial-polarization hyper-entangled states [33]. Our approach to polarization entanglement, utilizing C_3 rotational symmetry, is not limited to 3R-WS$_2$ and 3R-MoS$_2$ but is also applicable to other vdW materials. For example, tellurium, a chiral nonlinear crystal with a large $\chi^{(2)}$ and in-plane C_3 axis, shows promise for the generation and in-plane waveguiding of polarization-entangled photon pairs [34, 35]. These ultracompact entangled photon-pair sources will boost photonic quantum computation [9, 36, 37], quantum sensing [38] and super-resolution quantum imaging [10, 33].

Supplementary Information

The online version contains supplementary material available at https://doi.org/10.1186/s43593-024-00074-6.

> Additional file 1.

Author contributions
J.F., X.-F.R. and C.-W.Q. conceived and coordinated this work. J.F. prepared all samples for the measurements. Y.-K.W. and X.-F.R. designed and conducted the parametric down-conversion and quantum tomography experiments. R.D. and Z.L. synthesized the crystals. J.W. conducted the harmonic generation and reflectance spectroscopy measurements. J.F., Y.-K.W., X.-F.R., and C.-W.Q. drafted the paper with inputs from all authors. X.-F.R. and C.-W.Q. supervised the project.

Availability of data and materials
All data needed to evaluate the conclusions in this paper are available in the main text or the Supplementary Materials.

References

1. A. Zeilinger, Experiment and the foundations of quantum physics. Rev. Mod. Phys. **71**, S288–S297 (1999)
2. M. Erhard, M. Krenn, A. Zeilinger, Advances in high-dimensional quantum entanglement. Nat. Rev. Phys. **2**, 365–381 (2020)
3. P.G. Kwiat et al., New high-intensity source of polarization-entangled photon pairs. Phys. Rev. Lett. **75**, 4337–4341 (1995)
4. L. Li et al., Metalens-array–based high-dimensional and multiphoton quantum source. Science **368**, 1487–1490 (2020)
5. A. Mair, A. Vaziri, G. Weihs, A. Zeilinger, Entanglement of the orbital angular momentum states of photons. Nature **412**, 313–316 (2001)
6. J. Brendel, N. Gisin, W. Tittel, H. Zbinden, Pulsed energy-time entangled twin-photon source for quantum communication. Phys. Rev. Lett. **82**, 2594–2597 (1999)
7. Y. Wu et al., Optical spin–orbit interaction in spontaneous parametric downconversion. Optica **10**, 538–543 (2023)
8. J. Carolan et al., Universal linear optics. Science **349**, 711–716 (2015)
9. J. Wang, F. Sciarrino, A. Laing, M.G. Thompson, Integrated photonic quantum technologies. Nat. Photonics **14**, 273–284 (2020)
10. P.-A. Moreau, E. Toninelli, T. Gregory, M.J. Padgett, Imaging with quantum states of light. Nat. Rev. Phys. **1**, 367–380 (2019)
11. X. Xu et al., Towards compact phase-matched and waveguided nonlinear optics in atomically layered semiconductors. Nat. Photonics **16**, 698–706 (2022)
12. Q. Guo et al., Ultrathin quantum light source with van der Waals NbOCl2 crystal. Nature **613**, 53–59 (2023)
13. H. Hong et al., Twist phase matching in two-dimensional materials. Phys. Rev. Lett. **131**, 233801 (2023)
14. H. Zeng et al., Optical signature of symmetry variations and spin-valley coupling in atomically thin tungsten dichalcogenides. Sci. Rep. **3**, 1608 (2013)
15. K.L. Seyler et al., Electrical control of second-harmonic generation in a WSe2 monolayer transistor. Nat. Nanotechnol. **10**, 407–411 (2015)
16. H. Jin et al., On-chip generation and manipulation of entangled photons based on reconfigurable lithium-Niobate waveguide circuits. Phys. Rev. Lett. **113**, 103601 (2014)
17. Z. Ma et al., Ultrabright quantum photon sources on chip. Phys. Rev. Lett. **125**, 263602 (2020)
18. T. Stav et al., Quantum entanglement of the spin and orbital angular momentum of photons using metamaterials. Science **361**, 1101–1104 (2018)
19. T. Santiago-Cruz et al., Resonant metasurfaces for generating complex quantum states. Science **377**, 991–995 (2022)
20. Y. Tang et al., Harmonic spin–orbit angular momentum cascade in nonlinear optical crystals. Nat. Photonics **14**, 658–662 (2020)
21. H.J. Simon, N. Bloembergen, Second-harmonic light generation in crystals with natural optical activity. Phys. Rev. **171**, 1104–1114 (1968)
22. D.Y. Qiu, F.H. da Jornada, S.G. Louie, Optical spectrum of MoS2: many-body effects and diversity of exciton states. Phys. Rev. Lett. **111**, 216805 (2013)
23. A. Carvalho, R.M. Ribeiro, A.H. Castro Neto, Band nesting and the optical response of two-dimensional semiconducting transition metal dichalcogenides. Phys. Rev. B **88**, 115205 (2013)
24. Boyd, R. W. *Nonlinear Optics*. (Elsevier, 2003).
25. M.A. Weissflog et al., A tunable transition metal dichalcogenide entangled photon-pair source. Preprint at (2023). https://doi.org/10.48550/arXiv.2311.16036

26. V. Sultanov, T. Santiago-Cruz, M.V. Chekhova, Flat-optics generation of broadband photon pairs with tunable polarization entanglement. Opt. Lett. **47**, 3872–3875 (2022)
27. P.J. Mosley et al., Heralded generation of ultrafast single photons in pure quantum states. Phys. Rev. Lett. **100**, 133601 (2008)
28. U.A. Javid et al., Ultrabroadband entangled photons on a nanophotonic chip. Phys. Rev. Lett. **127**, 183601 (2021)
29. A. Politi, M.J. Cryan, J.G. Rarity, S. Yu, J.L. O'Brien, Silica-on-silicon waveguide quantum circuits. Science **320**, 646–649 (2008)
30. A. Peruzzo et al., Quantum walks of correlated photons. Science **329**, 1500–1503 (2010)
31. X.-M. Jin et al., Experimental free-space quantum teleportation. Nat. Photonics **4**, 376–381 (2010)
32. R. Verre et al., Transition metal dichalcogenide nanodisks as high-index dielectric Mie nanoresonators. Nat. Nanotechnol. **14**, 679–683 (2019)
33. H. Defienne, B. Ndagano, A. Lyons, D. Faccio, Polarization entanglement-enabled quantum holography. Nat. Phys. **17**, 591–597 (2021)
34. Q. Fu et al., Berry curvature dipole induced giant mid-infrared second-harmonic generation in 2D Weyl semiconductor. Adv. Mater. **35**, 2306330 (2023)
35. M. Suárez-Rodríguez et al., Odd nonlinear conductivity under spatial inversion in chiral tellurium. Phys. Rev. Lett. **132**, 046303 (2024)
36. E. Pelucchi et al., The potential and global outlook of integrated photonics for quantum technologies. Nat. Rev. Phys. **4**, 194–208 (2022)
37. L. Feng et al., Silicon photonic devices for scalable quantum information applications. Photonics Res. **10**, A135–A153 (2022)
38. C.L. Degen, F. Reinhard, P. Cappellaro, Quantum sensing. Rev. Mod. Phys. **89**, 035002 (2017)